Canadian Journal of
Neurological Sciences
Journal Canadien des
Sciences Neurologiques

Original Article

Brain Imaging Abnormalities in Mixed Alzheimer's and Subcortical Vascular Dementia

Hyunwoo Lee[1] (iD), Vanessa Wiggermann[2], Alexander Rauscher[2], Christian Kames[2], Mirza Faisal Beg[3], Karteek Popuri[3,4],
Roger Tam[5], Kevin Lam[5], Claudia Jacova[6], Elham Shahinfard[2], Vesna Sossi[2], Jacqueline A. Pettersen[1] and
Ging-Yuek Robin Hsiung[1]

[1]Division of Neurology, Department of Medicine, University of British Columbia, Vancouver, BC, Canada, [2]Department of Physics & Astronomy, University of
British Columbia, Vancouver, BC, Canada, [3]School of Engineering Science, Simon Fraser University, Burnaby, BC, Canada, [4]Department of Computer Science,
Memorial University of Newfoundland, St. John's, NL, Canada, [5]Department of Radiology and MS/MRI Research Group, University of British Columbia, Vancouver,
BC, Canada and [6]School of Graduate Psychology, Pacific University, Hillsboro, OR, USA

ABSTRACT: *Background:* A large proportion of Alzheimer's disease (AD) patients have coexisting subcortical vascular dementia (SVaD), a condition referred to as mixed dementia (MixD). Brain imaging features of MixD presumably include those of cerebrovascular disease and AD pathology, but are difficult to characterize due to their heterogeneity. *Objective:* To perform an exploratory analysis of conventional and non-conventional structural magnetic resonance imaging (MRI) abnormalities in MixD and to compare them to those observed in AD and SVaD. *Methods:* We conducted a cross-sectional, region-of-interest-based analysis of 1) hyperintense white-matter signal abnormalities (WMSA) on T2-FLAIR and hypointense WMSA on T1-weighted MRI; 2) diffusion tensor imaging; 3) quantitative susceptibility mapping; and 4) effective transverse relaxation rate (R2*) in N = 17 participants (AD:5, SVaD:5, MixD:7). General linear model was used to explore group differences in these brain imaging measures. *Results:* Model findings suggested imaging characteristics specific to our MixD group, including 1) higher burden of WMSAs on T1-weighted MRI (versus both AD and SVaD); 2) frontal lobar preponderance of WMSAs on both T2-FLAIR and T1-weighted MRI; 3) higher fractional anisotropy values within normal-appear white-matter tissues (versus SVaD, but not AD); and 4) lower R2* values within the T2-FLAIR WMSA areas (versus both AD and SVaD). *Conclusion:* These findings suggest a preliminary picture of the location and type of brain imaging characteristics associated with MixD. Future imaging studies may employ region-specific hypotheses to distinguish MixD more rigorously from AD or SVaD.

RÉSUMÉ : Anomalies de l'imagerie du cerveau dans la maladie d'Alzheimer et la démence vasculaire sous-corticale mixte. *Contexte :* Une bonne proportion de patients atteints de la maladie d'Alzheimer (MA) souffrent également de démence vasculaire sous-corticale (DVSC), affection appelée *démence mixte* (DM). Les manifestations de la DM à l'imagerie du cerveau comprennent probablement celles de la maladie vasculaire cérébrale et de la MA, mais elles sont difficiles à caractériser en raison de leur hétérogénéité. *Objectif :* L'étude visait à réaliser une analyse préliminaire des anomalies structurales courantes et non courantes, observées à l'imagerie par résonance magnétique (IRM) du cerveau dans la DM, et à comparer les anomalies observées dans la MA et la DVSC. *Méthode :* Pour ce faire, nous avons procédé à une analyse transversale : 1) des anomalies de signal de la substance blanche (ASSB) de type hyperintense à la séquence FLAIR en T2 et des ASSB de type hypointense à l'IRM pondérée en T1; 2) de l'imagerie en tenseur de diffusion; 3) de la cartographie de susceptibilité quantitative; 4) de la vitesse de relaxation transversale vraie (R2*) chez 17 participants (MA : 5; DVSC : 5; DM :7), dans des régions présentant un intérêt particulier. Un modèle linéaire général a servi à examiner les différences de mesures observées à l'imagerie du cerveau, entre les groupes. *Résultats :* D'après les résultats du modèle, il se dégagerait de l'imagerie des caractéristiques propres au groupe de DM étudié, notamment : 1) une charge d'ASSB plus élevée à l'IRM pondérée en T1 (que dans la MA et la DVSC); 2) une prédominance des ASSB provenant du lobe frontal, tant à la séquence FLAIR en T2 qu'à l'IRM pondérée en T1; 3) des valeurs d'anisotropie fractionnelle plus élevées dans les tissus de substance blanche d'apparence normale (que dans la DVSC mais pas dans la MA); 4) des valeurs R2* plus faibles dans les régions d'ASSB à la séquence FLAIR en T2 (que dans la MA et la DVSC). *Conclusion :* Les résultats permettent de dégager un tableau préliminaire du siège des caractéristiques de l'imagerie du cerveau, et de leur type, associées à la DM. Il serait donc justifié de poursuivre les études sur l'imagerie du cerveau, fondées sur des hypothèses ciblant des régions particulières afin de distinguer de manière plus rigoureuse la DM de la MA ou de la DVSC.

Introduction

Alzheimer's disease (AD) and vascular dementia (VaD) represent the leading causes of dementia, accounting for around 60-80% and 15% of all dementia cases, respectively.[1,2] AD is characterized by the accumulation of misfolded amyloid-beta protein (Aβ plaques) and aggregation of tau protein (neurofibrillary tangles), which cause neurodegenerative changes that lead to memory deficits and executive dysfunctions as well as language, attention, or visuo-spatial impairments.[3] By contrast, VaD is linked to variable cognitive impairments that depend on the specific sites and type of apparent cerebrovascular pathology.[2] The most common type is subcortical vascular dementia (SVaD), which is characterized by steno-occlusion of small vessels leading to ischemic white-matter (WM) lesions and subcortical lacunar infarctions.[2,4]

Yet, evidence suggests that a large proportion of dementia cases are associated with multiple underlying pathologies and therefore cannot be identified as either purely AD or SVaD. Rather, they are referred to as "mixed" dementia (MixD) with the most common form being the coexistence of AD and vascular pathologies that exacerbates with age.[5,6] For example, prospective amyloid imaging studies leveraging 11C-labeled Pittsburgh compound-B positron emission tomography (PiB-PET; an in vivo molecular imaging of Aβ) have found PiB positivity in ∼30% of SVaD participants.[7,8] The presence of mixed AD and vascular pathologies has also been confirmed in a series of autopsy studies, including the Nun Study (39% of AD cases had at least one infarct),[9] the Rochester Epidemiology Project (12% of dementia cases had combined AD and VaD),[10] the Rush Religious Orders Study and the Memory and Aging Project (38% of dementia cases had mixed AD and cerebral infarctions[11]; 30.2% of probable AD cases had mixed AD and macroscopic infarcts[12]), Jellinger and colleagues (16–20% of AD cases had additional cerebrovascular lesions),[13] the Baltimore Longitudinal Study of Aging (35% of dementia cases associated with hemispheral infarcts alone or in conjunction with AD pathology),[14] the Hisayama Study (7.9% of dementia cases had neuropathological diagnosis of AD + VaD),[15] the Honolulu-Asia Aging Study (14.2% of dementia cases had mixed Alzheimer and microvascular ischemic lesions),[16] and De Reuck and colleagues (30% of dementia cases had mixed AD and cerebrovascular lesions).[17] These findings suggest that dementia cases with mixed pathologies are relatively common.

Previous studies have shown different patterns of neuropsychological and neuropsychiatric outcomes among AD, SVaD, and suspected MixD subjects who were stratified based on clinical and imaging features (i.e. by means of fulfilling the diagnostic criteria of both AD and SVaD and/or having SVaD with amyloid positivity). For example, MixD performed significantly worse in global cognitive composite, attention, and visuo-construction scores compared to AD,[18] as well as significantly worse in memory tasks compared to SVaD.[7] Also, MixD showed less depressive symptoms and aberrant motor behaviors compared to VaD, but had marginally more agitation compared to AD.[19] Therefore, although autopsy findings are essential to confirm the presence of mixed pathology, a biomarker-based characterization of the clinically defined population may help us distinguish suspected MixD from AD or SVaD.

To date, various magnetic resonance imaging (MRI) contrasts have been applied to characterize brain abnormalities associated with AD and VaD. For example, MRI-based morphometric studies have shown that AD is typically associated with atrophy of the medial temporal lobe structures (e.g. hippocampus and entorhinal cortex), temporal and parietal lobes as well as subcortical nuclei.[3]

In SVaD, the hippocampus and entorhinal cortex are less affected compared to AD although substantial cortical thinning can be found in the frontal and temporal lobe areas.[20,21] The primary MRI feature of SVaD is considered to be WM signal abnormalities (WMSA), visible as hyperintensities on T2-weighted or fluid-attenuated inversion recovery (T2-FLAIR) images, which presumably represent small vessel disease associated with chronic ischemia.[22] However, T2-hyperintense WMSA (T2-HyperWMSA) are also present in AD, especially around the parietal and occipital periventricular regions.[23,24] Furthermore, non-conventional MRI techniques have been used to compare microstructural tissue properties in AD and VaD. For example, diffusion tensor imaging (DTI) studies have observed lower fractional anisotropy (FA; the degree of anisotropic water diffusion) and higher mean diffusivity (MD; the magnitude of water diffusion) values in most WM tracts in SVaD compared to AD.[25,26] Recent studies have also investigated magnetic susceptibility alterations by means of quantitative susceptibility mapping (QSM), where elevated QSM levels were found in early AD and in VaD compared to controls especially within the subcortical nuclei structures.[27–31] Such increased susceptibility measurements may be explained by demyelination and increased iron concentrations,[27,29–33] which may result from iron misregulation, accumulation, or neuronal loss during neurodegenerative pathogenesis.[34,35]

Nonetheless, brain abnormalities in individuals with suspected MixD remain to be elucidated. Conventional MRI findings suggest that global measures such as whole-brain volume, gray matter (GM) volume, or WM hyperintensities count/volume may not be well-suited for differentiating MixD from AD or SVaD as they share similar imaging features.[36,37] AD-specific changes in subcortical structures (e.g. hippocampal and amygdala shapes) may distinguish MixD from SVaD,[8] but not from AD. Likewise, changes in WM tracts (e.g. DTI indices) may differentiate MixD from AD,[38] but not from SVaD. Moreover, the scarcity of MixD imaging studies is likely due to the difficulty in recruiting appropriate participants, who are likely among the oldest of the old and are unlikely to tolerate MRI and/or PiB-PET sessions. This highlights the significance of well-focused hypotheses and careful selection of MRI contrasts and methods especially relevant to MixD.

We conducted an exploratory study to assess potential brain abnormalities in mixed dementia using conventional and non-conventional MRI measures sensitive to changes in brain tissue properties. To investigate, we analyzed participants recruited at a single site who were classified in terms of clinical diagnosis of AD, SVaD, or MixD (i.e. fulfilling the diagnostic criteria of both AD and SVaD). We hypothesized that our MixD group would have characteristic MRI abnormalities due to contributions from both AD and SVaD pathologies. To investigate, we conducted region-of-interest (ROI)-based comparisons of MixD with either AD or SVaD in terms of 1) conventional measures including WMSA and DTI parameters as well as 2) novel susceptibility-weighted imaging-based metrics including QSM) and effective transverse relaxation rate (R2*). Our findings can provide a priori knowledge for future studies of imaging abnormalities in MixD.

Methods

Study Participants

A total of 17 participants were recruited through the University of British Columbia Clinic for Alzheimer's Disease and Related

Table 1: Baseline demographic, clinical, cognitive, and global brain volume characteristics for in AD, MixD, and SVaD subjects

Diagnosis subgroup		Alzheimer's disease (AD)	Mixed Alzheimer's and subcortical vascular dementia (MixD)	Subcortical vascular dementia (SVaD)
N (total N = 17)		5	7	5
Demographic	Age (mean, (SD))	72.2 (11.0)	78.7 (5.3)	71.9 (6.6)
	Sex (F:M)	1:4	2:5	3:2
	Education years (mean, (SD))	16.6 (2.8)	14.3 (2.2)	13.4 (3.4)
Clinical	Years from symptoms onset to MRI date (mean, (SD))	6.2 (2.2)	5.0 (2.6)	4.4 (3.2)
	Hypertension, yes (N)	1	2	2
	Dyslipidemia, yes (N)	1	0	0
	Smoking, yes (N)	3	5	0
	Type-2 Diabetes, yes (N)	1	2	1
	CDRSOB (median, [range])	5 [3.5–11]	5.5 [3.5–11]	1.5 ** [1–3.5]
	NPI Total (median, [range])	8 [0–27]	7 [1–14]	3 [0–21]
	FAQ Total (median, [range])	17 [11–25]	16 [11–21]	9 *** [1–13]
	GDS Total (median, [range])	2 [1–3]	2 [1–8]	2 [1–9]
	FTT Average Dominant (median, [range])†	41 [15, 59]	31 [18, 42]	27 [15, 47]
	FTT Average Non-Dominant (median, [range])†	39 [15, 54]	26 [12, 45]	18 [6, 39]
	MOT Mean Latency (median, [range])††	−1.5 [−2.4, 1.1]	−0.7 [−1.1, 0.2]	−0.6 [−1.4, 0.14]
	MOT Mean Error (median, [range])††	0.2 [−0.2, 0.4]	0.3 [0.1, 0.4]	0.06 [−0.4, 0.1]
Cognition	MoCA Total (median, [range])	19 [18–23]	16 [12–21]	22 [15–28]
	MMSE Total (median, [range])	24 [20–27]	24 [21–28]	25 [21–28]
Global brain volume at baseline, adjusted for head size [% of intracranial volume] (mean, (SD))	Whole Brain	65.8 (4.0)	63.8 (4.0)	67.4 (5.0)
	Cortical Gray Matter	26.7 (1.0)	26.3 (1.2)	28.4 (2.4)
	Total White Matter	27.2 (3.1)	25.9 (3.1)	26.9 (3.8)

CDRSOB, Clinical Dementia Rating Scale Sum of Boxes; NPI, Neuropsychiatric Inventory; FAQ, Functional Activities Questionnaire; GDS, Global Deterioration Scale; FTT, Finger Tapping Test; MOT, Motor Screening Task Standard Score; MoCA, Montreal Cognitive Assessment; MMSE, Mini-Mental State Exam.
† FTT: 1 MixD missing.
†† MOT: 2 MixD, 1 SVaD missing.
* Neither age, age, education level, NPI, GDS, FTT, MOT, MoCA, MMSE nor baseline level of atrophy (whole-brain, cortical GM, and total WM) were significantly different among AD, SVaD, and MixD.
** SVaD had significantly lower CDRSOB scores compared to AD ($p = 0.05$) or MixD ($p = 0.03$), ANOVA and Tukey's HSD post hoc testing.
*** SVaD had significantly lower FAQ total scores compared to AD ($p = 0.01$) or MixD ($p = 0.01$), ANOVA, and Tukey's HSD post hoc testing.

Disorders. The participants were stratified into probable AD if they fulfilled the McKhann NIA-AA criteria,[39] or SVaD if they fulfilled the criteria by Erkinjuntti,[40] or into the MixD subgroup if they fulfilled the diagnostic criteria of both AD and SVaD. This study was approved by the University of British Columbia Clinical Ethics Review Board. All experiments were performed in accordance with relevant guidelines and regulations. All participants provided written informed consent. Table 1 summarizes the baseline demographic, clinical, cognitive, and global brain volume characteristics for each diagnostic subgroup. We report the following global measures of clinical and cognitive functions: Clinical Dementia Rating Sum of Boxes (CDRSOB), Neuropsychiatric Inventory (NPI), Functional Activities Questionnaire (FAQ), Global Deterioration Scale (GDS), Finger Tapping Test (FTT), Motor Screening Task Standard Score (MOT), Montreal Cognitive Assessment (MoCA), and Mini-Mental State Exam (MMSE) total scores.

Image Acquisition

Participants were cross-sectionally scanned on a 3.0 T Philips Achieva MRI scanner (all N = 17 participants) and a GE

Table 2: PET and MRI acquisition protocols

Imaging sequence	Parameters
11C-Pittsburgh compound-B positron emission tomography (PiB-PET)	11C-Pittsburgh Compound-B (PiB) produced at UBC TRIUMF. In-plane resolution = 2.3 mm; Slice thickness = 1.2mm 90-min dynamic acquisition time, data framed into $18 \times 300s$ sequence.
3D T1-weighted turbo field echo (T1-TFE)	Axial, TR/TE (ms) = 7.8/3.6, 256×200 matrix, 170 partitions, 8 degrees flip angle; Coronal 3D T1-weighted scan: Matrix = $256 \times 256 \times 160$, voxel size $1 \times 1 \times 1$ mm^3, TR = 8.1 ms, TE = 3.7 ms. Flip angle = 6 degrees.
T2-weighted fluid attenuation inversion recovery (T2-FLAIR)	Axial, TR/TI (ms) = 11,000/2800, TE(ms) = 125, Matrix = $256 \times 256 \times 60$, voxel size $1 \times 1 \times 3$ mm^3
Diffusion tensor imaging (DTI)	60 directions, b0 = 0, b1 = 700, Matrix = 100×100, Field of View = 224×224, Voxel size = $2.2 \times 2.2 \times 2.2$ mm^3, 70 slices, TR = 7015 ms, TE = 60 ms, flip angle = 90 degrees.
Multi-echo susceptibility-weighted imaging (SWI) with 5 Echoes	Axial 3D multi-echo sequence with Matrix = $440 \times 222 \times 64$; Field of View = $220 \times 167 \times 128$ mm^3, Voxel size = $0.5 \times 0.75 \times 2$ mm^3 and reconstructed to $0.5 \times 0.5 \times 1$ mm^3, TR = 30 ms, TE = 5, 10, 15, 20, 25 ms. Flip angle = 17 degrees.

Advance PET tomography (N = 15 due to two participants not consenting to PET scanning). Two PiB-PET data sets were further excluded from subsequent analysis due to low tracer dose or motion artifact (final PET N = 13; 4:5:4 AD:MixD:SVaD). The acquired sequences are outlined in Table 2.

PET Processing

Reconstructed PET imaging data were frame-to-frame realigned and motion-corrected using AIR.[41] A PiB-PET template in the Montreal Neurological Institute (MNI) 305 space was created by averaging a set of PiB-PET images from a separate cohort of healthy control subjects whose MRI images had been warped to the SPM MNI305 template. For each subject, the mean PiB-PET image was normalized to the PiB-PET template via non-linear regularization (16 non-linear iterations and 8 mm smoothing) and affine regularization. Then, all the PiB-PET frames were transformed to the MNI space using the corresponding parameters. Standardized uptake value ratio (SUVR) 40 to 90 min post-injection was calculated by normalizing SUV (tracer concentration/(injected dose/body weight)) images to the cerebellar cortex SUV.

To explore the distribution of Aβ on PET among our participants, we calculated the average SUVR (for minutes 40 to 90) within the following bilateral ROIs grouped by cortical and subcortical regions: frontal (orbitofrontal and medial prefrontal cortex), parietal (angular gyrus, superior parietal, precuneus, and supramarginal gyrus), temporal (lateral temporal gyrus, middle temporal gyrus, medial temporal gyrus, and temporal pole), occipital (occipital cortex, medial occipital), sensory-motor cortex, cingulate gyrus (posterior and anterior cingulate gyrus), perirolandic region, and subcortical nuclei (thalamus, caudate and putamen).

MRI Processing – Preprocessing of T1-Weighted Images

T1-weighted images were visually checked for quality and then processed using the FreeSurfer 6.0 cross-sectional pipeline, which provides cortical reconstruction and volumetric segmentation.[42,43] We utilized a version implemented in the "Cloud Engine Resource for Accelerated Medical Image Computing for Clinical Applications" (CERAMICCA; https://ceramicca.ensc.sfu.ca) portal. All FreeSurfer outputs were manually examined and corrected for errors.

The outputs from the FreeSurfer volumetric pipeline were used to obtain the whole-brain, cortical GM, and total WM volumes for each participant. Further, FreeSurfer-derived subcortical GM nuclei and hippocampal/amygdala volumetric outputs were combined with the large deformation diffeomorphic metric mapping (LDDMM[44])-based label propagation method[45] to produce segmentations of subcortical structures (caudate, putamen, pallidus, thalamus, and hippocampus/amygdala) for each participant. To account for individual variations in head size, we also calculated total intracranial volume (ICV) for each participant using a multi-atlas label fusion method.[46]

MRI Processing – WM Structural Abnormalities

T2-HyperWMSA were identified on T2-FLAIR images using in-house software based on the following steps: 1) manual identification of pathological hyperintensities by a neuroradiologist, who marked each lesion with one or more seed points, 2) intensity thresholding based on T2-FLAIR signal intensity distribution, 3) removal of hyperintensities not containing any seed points. While the lesion identification step was manual, the rest was automated. For each participant, the T2-FLAIR image and the T2-HyperWMSA mask were 6-parameter rigid body registered to the T1-weighted scan using FSL-FLIRT.[47]

T2-HyperWMSA that also appear hypointense on the corresponding T1-weighted image (i.e. T1-HypoWMSA) are considered as areas of more severe WM injury, as suggested by more aberrant DTI values and their association with faster conversion from mild cognitive impairment (MCI) to AD.[48,49] We additionally identified T1-HypoWMSA on T1-weighted images as markers that may be more specific to tissue damage in the WM. They were defined for each participant as follows: The voxels within the T2-HyperWMSA mask with the corresponding T1-weighted image intensity of 65% or lower than the surrounding normal-appearing white-matter (NAWM) voxels.

The burden and distribution of WMSAs were assessed in terms of ROIs, which included total and lobar (frontal, parietal, occipital, and temporal) WM masks. The lobar ROIs were defined on T1-weighted images by combining the corresponding Desikan-Killiany atlas labels through FreeSurfer's "mri_annotation2label" and "mri_aparc2aseg" functions.[50] For each ROI, we obtained the ICV-normalized volume of T2-HyperWMSA

(i.e. (T2-HyperWMSA∩ROI voxels) over (ICV voxels) * 100), which was used as an index of apparent WM tissue abnormalities within the specific ROI. The same was repeated for T1-HypoWMSA.

For further analyses, we defined normal-appearing gray matter (NAGM) and white-matter (NAWM) ROIs as follows: 1) segmentation of GM and WM on T1-weighted images using SPM12 (https://www.fil.ion.ucl.ack.uk/spm/), 2) creation of GM and WM masks using binarization threshold of >0.5, and 3) subtraction or addition of the T2-HyperWMSA mask from the GM and WM masks, respectively.

DTI images were processed using the FSL Diffusion Toolbox.[51,52] Briefly, the steps included 1) manual checking of the diffusion data, 2) susceptibility-induced distortion correction using "topup", 3) brain extraction on the corrected non-diffusion weighted b0 images using "bet," 4) eddy currents and subject motion correction using "eddy," and 5) voxel-wise fitting of the eddy-corrected diffusion tensor data using "dtifit."

For comparison, we assessed the average FA and MD values within major WM tracts based on the ICBM-DTI-81 WM labels atlas.[53] While the atlas comprises 48 WM tract labels, they were combined to reduce the number of comparisons. However, we assessed the regions overlapping with T2-HyperWMSA and the normal-appearing regions separately, in order to detect differences in WM microstructure that are not captured by WM hyperintensities.

MRI Processing – QSM and R2*

SWI images were processed using in-house software to produce maps of QSM as well as R2*, which is a related measure that is correlated with iron in deep GM and myelin and iron in WM.[54,55] QSM was reconstructed using a rapid two-step dipole inversion algorithm.[55] Maps of R2* relaxation rates were computed by fitting a mono-exponential decay function to the multi-echo data[56] after correction for signal decay due to background inhomogeneities.[57]

We evaluated the average QSM and R2* values within the predefined T2-HyperWMSA and T1-HypoWMSA ROIs as well as within major subcortical nuclei (caudate, putamen, pallidus, thalamus, hippocampus, and amygdala). For this, the WMSAs and the FreeSurfer+LDDMM-derived subcortical nuclei ROIs were 6-parameter rigid body registered to the corresponding SWI images.

Statistical Analysis

All analyses were conducted using SAS PROC GLM and JMP software (SAS, Cary, NC). Analysis of variance (ANOVA) and Tukey's HSD post hoc tests were used to identify differences between groups in age, education, CDRSOB, NPI, FAQ, GDS, MoCA, MMSE, and baseline global brain volume measures.

Due to the further reduced sample size in our PiB-PET analysis, we did not conduct formal statistical analyses. Instead, we reported the individual SUVR data within the 19 predefined ROIs with a reference threshold to determine PiB-PET positivity within the region. As our PET imaging protocol followed that of the Alzheimer's Disease Neuroimaging Initiative (ADNI), we provided an ADNI literature threshold of 1.465.[58]

T2-HyperWMSA, T1-HypoWMSA, and SWI measures were analyzed using a GLM to assess subgroup differences while adjusting for age and sex (model: MRI_measure ~ subgroup + age + sex). DTI-based measures were analyzed using a similar GLM with additional ICV-corrected WM volume term to account for the

effect of atrophy (model: MRI_measure ~ subgroup + age + sex + volume). Similar as above, we examined whether the omnibus F-test was significant and then used Dunnett's test to conduct post hoc multiple comparisons with MixD as the control group (2 total: MixD vs. AD; MixD vs. SVaD).

Additionally, DTI, QSM, and R2* measures were analyzed using two-tailed paired t-tests to assess differences in values between normal-appearing and WMSA areas (T2-HyperWMSA for DTI; T2-HyperWMSA and T1-HypoWMSA for QSM and R2*).

Correction for multiple comparisons: For the GLM analyses, we have used a hierarchical approach where we first performed the omnibus F-test to assess whether a group difference exists in a given measure among MixD, AD, and SVaD. If the omnibus test was not significant, we stopped the analysis as there was no evidence of rejecting the null hypothesis. However, if the omnibus test was significant (F-statistic < 0.05), we proceeded with post hoc pairwise group comparisons using Dunnett method with MixD as the control group. Two comparisons were made against MixD (MixD vs. AD and MixD vs. SVaD), with the p-values adjusted for multiple comparisons. We assumed that the dependent variables (multi-modal MRI measures) were strongly correlated with each other, as they were each acquired from the same participant. For the paired t-tests, we have used the Bonferroni method to adjust the p-values for the simultaneous pairwise comparisons (WMSA vs. normal-appearing WM for each group, leading to 3 comparisons per measure). We assumed that the comparisons were independent, resulting in the significance threshold of p = 0.004.

Results

Baseline Characteristics

Our MixD participants tended to have older age and lower MoCA scores than the other participants, although not statistically significant. Overall, neither age, education level, NPI, GDS, FTT, MOT, MoCA, MMSE nor baseline level of atrophy (whole-brain, cortical GM, and total WM) were significantly different among the subgroups. However, both AD and MixD had significantly higher CDRSOB and FAQ total scores compared to SVaD participants. Table 1 summarizes the findings.

Description of PiB-PET SUVR Data

Figure 1 presents the individual PiB-PET SUVR data in the 19 ROIs, grouped by cortical and subcortical regions. AD participants had above-threshold SUVR in most regions, except in the temporal pole, perirolandic, medial occipital, and medial temporal regions. The majority of MixD participants (60-80%) had above-threshold SUVR in all regions, except in the temporal pole, medial temporal, and occipital regions. The proportion of above-threshold SVaD participants was relatively more varied and region-dependent.

MRI Results – White-Matter Hyperintensities and Hypointensities

Figure 2 provides representative FLAIR images depicting the presence of brain atrophy and WM hyperintensities in the AD, SVaD, and MixD participants. T2-HyperWMSA proportions, adjusted for age and sex, were significantly higher in the MixD subgroup versus the AD subgroup (p = 0.0067) but not versus the SVaD subgroup (p = 0.11). Assessing the regional distribution, the effect was significant in the frontal lobe (MixD vs. AD p = 0.0094; MixD vs.
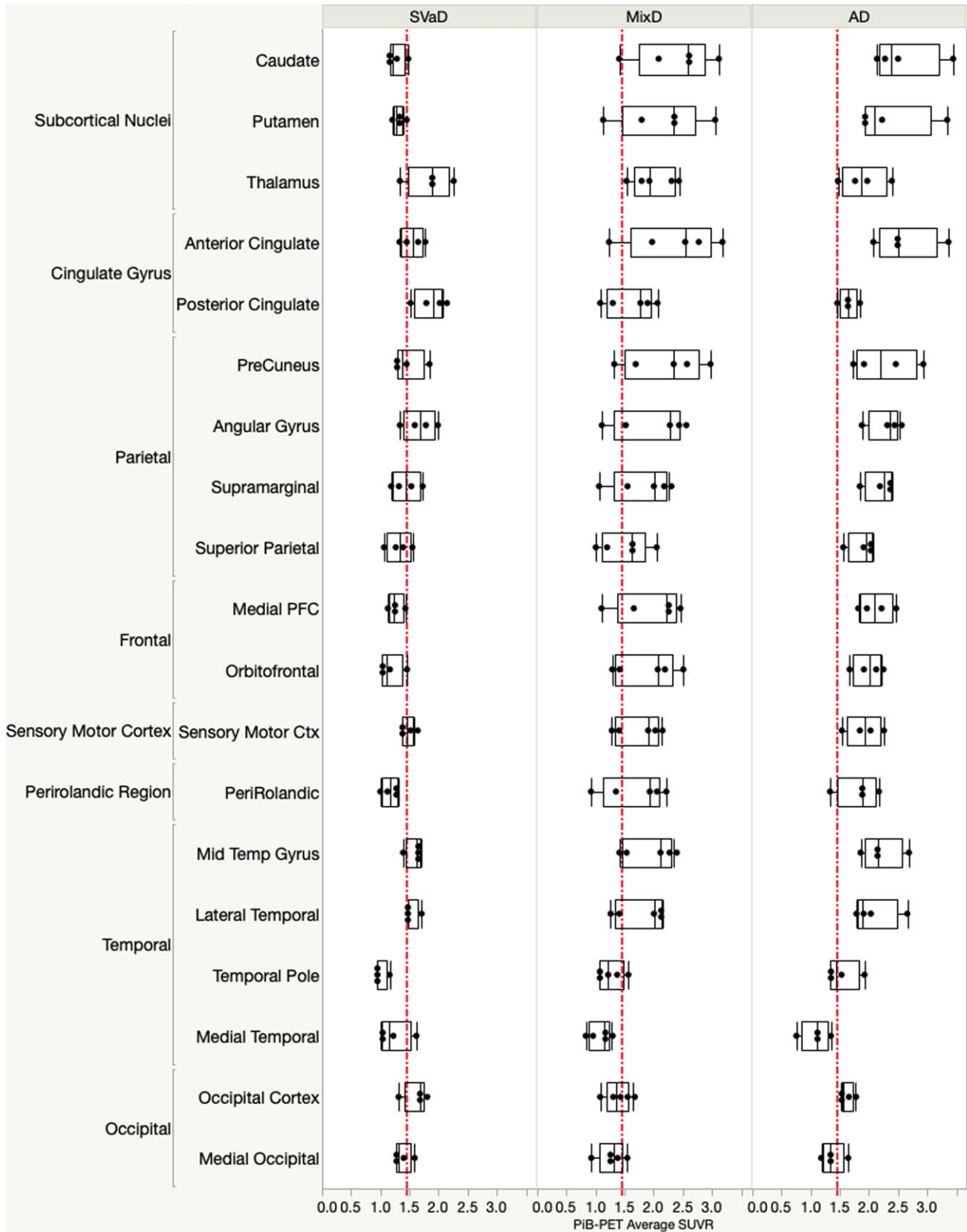
Figure 1: PiB-PET average SUVR data in the 19 ROIs, grouped by cortical and subcortical regions. Each data point represents each individual participant, with boxplots showing quantile statistics. Red dashed lines represent the PET positivity threshold of 1.465.
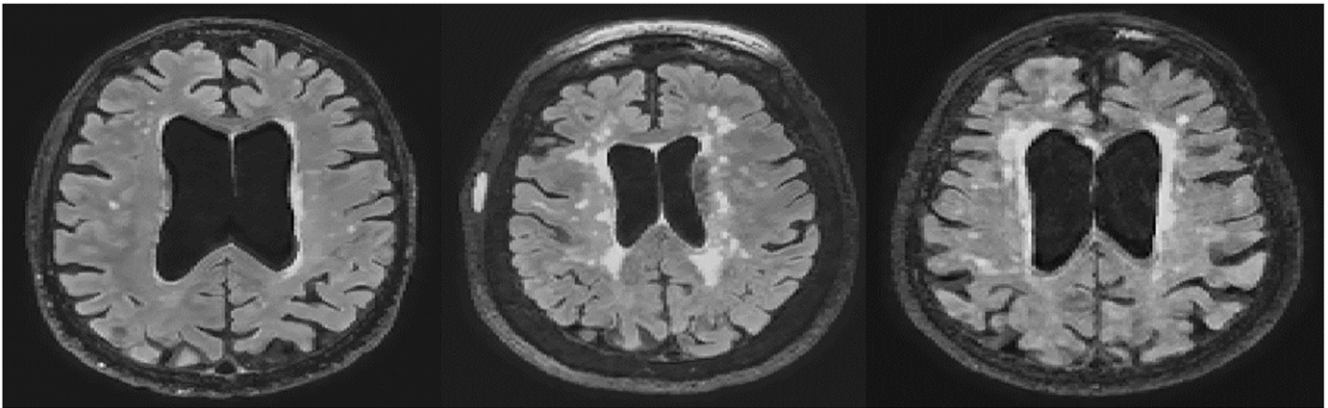
Figure 2: Examples of the T2-FLAIR image for AD (Left), SVaD (Middle), and MixD (Right) that demonstrates the presence of brain atrophy and white-matter signal abnormalities (hyperintensities).

SVaD $p = 0.07$) and the occipital lobe (MixD vs. AD $p = 0.026$; MixD vs. SVaD $p = 0.92$) but not in the other lobes.

T1-HypoWMSA proportions were significantly higher in the MixD subgroup versus both the AD ($p = 0.01$) and the SVaD ($p = 0.04$) subgroups. The effect was dominant in the frontal lobe (MixD vs. AD $p = 0.02$; MixD vs. SVaD $p = 0.02$) but not in the other lobes. Table 3 compares the ICV-adjusted volumes of T2-HyperWMSA and T1-HypoWMSA among the subgroups and provides post hoc findings for significant comparisons. Figure 3 shows the frequency maps of WM hyperintensities (T2-HyperWMSA) that have been normalized to the MNI 152 template for easier visualization.

MRI Results – White-Matter DTI

Comparisons among AD, SVaD, and MixD: Significant subgroup effects in FA and MD values were noted within the total and NAWM tracts. Within both ROIs, the SVaD subgroup had significantly lower FA values versus MixD (total: $p = 0.017$; normal-appearing: $p = 0.0082$) while the AD and MixD comparison was not significant (total: $p = 0.36$; normal-appearing: $p = 0.91$). MD values were not significantly different among the subgroups. Table 4 compares the FA and MD values among the subgroups and provides post-hoc findings for significant comparisons.

Comparisons between normal-appearing and WMSA areas: For MixD, paired Bonferroni-corrected t-tests indicated significantly lower FA ($p < 0.0003$) and higher MD ($p < 0.002$) values within T2-HyperWMSA versus NAWM. For SVaD, T2-HyperWMSA had significantly lower FA ($p = 0.01$) but comparable MD ($p = 0.17$) values compared to NAWM. For AD, both FA ($p = 0.53$) and MD ($p = 1.0$) values were not significantly different between T2-HyperWMSA and NAWM.

MRI Results – White-Matter and Subcortical Nuclei SWI

Comparisons among AD, SVaD, and MixD: QSM values within the assessed ROIs were not significantly different among the subgroups. However, R2* measures within the T2-HyperWMSA areas were significantly lower in the MixD subgroup versus both AD ($p = 0.03$) and SVaD ($p = 0.04$). Other regions showed insignificant differences. Table 5 compares the QSM and R2* values among the subgroups and provides post hoc findings for significant comparisons. Figure 4 shows the examples of the QSM and R2* images with the subcortical nuclei ROI masks overlaid.

Comparisons between normal-appearing and WMSA areas: Paired Bonferroni-corrected t-tests indicated nonsignificant difference in susceptibility (AD $p = 1.0$; MixD $p = 1.0$; SVaD $p = 1.0$) but significantly lower R2* (AD $p = 0.0015$; MixD $p < 0.0003$; SVaD $p < 0.0003$) values within T2-HyperWMSA versus NAWM. Results were similar between T1-HypoWMSA and NAWM (susceptibility: AD $p = 0.17$; MixD $p = 0.16$; SVaD $p = 0.52$; R2*: AD $p = 0.009$; MixD $p < 0.0003$; SVaD $p < 0.0003$).

Discussion

We conducted an exploratory analysis of brain imaging abnormalities in clinically diagnosed MixD, AD, and SVaD participants in terms of ROI-based comparisons of conventional and non-conventional MRI metrics. PiB-PET positivity was observed within the AD-relevant regions for most MixD and AD participants. MRI characteristics of our MixD participants included 1) significantly higher proportion of WM structural abnormalities, mainly within the frontal lobe, as indicated by T2-HyperWMSA (versus AD) or T1-HypoWMSA (versus AD and SVaD); 2) significantly higher DTI FA values within major NAWM tracts versus SVaD, but not versus AD; and 3) significantly lower R2* values within the T2-HyperWMSA areas compared to both AD and SVaD.

Overview of PiB-PET SUVR Data

We used PiB-PET SUVR to explore the regional distribution of Aβ pathology among our study participants, who were stratified based on clinical diagnostic criteria.[39,40] It is recognized that in AD, 11C-PiB radiotracer binding is consistently elevated in regions including the prefrontal cortex, precuneus, posterior cingulate cortex, lateral parietal cortex, lateral temporal cortex, and striatum.[59–61] Indeed, all of AD and most (60–80%) of MixD participants had SUVR above the threshold in all of those regions. SVaD participants had relatively lower uptake level in the AD-related regions, except for posterior cingulate cortex and angular gyrus. This may be consistent with an increased PiB-uptake level in the precuneus and posterior cingulate cortex observed in patients after subcortical ischemic stroke.[62] Furthermore, elevated posterior cingulate and occipital uptake level may indicate an occipital-predominant pattern observed in SVaD,[63] although this needs to be verified in future work with larger samples.

Table 3: Proportions of FLAIR white-matter hyperintensities (T2-HyperWMSA) and T1w-hypointensities (T1-HypoWMSA) within total white-matter and bilateral lobar regions of interest

Measure	ROI	Subgroup mean±SD			Pairwise post hoc comparisons p-value *
		AD	MixD	SVaD	
T2-HyperWMSA, adjusted for ICV volume [% of ICV]	Total white matter	**0.31** (0.27)	**2.31** (1.16)	**1.43** (1.00)	MixD vs. SVaD: 0.11 **MixD vs. AD: 0.0067**
	Frontal lobe	**0.11** (0.13)	**1.19** (0.70)	**0.65** (0.56)	MixD vs. SVaD: 0.07 **MixD vs. AD: 0.0094**
	Parietal lobe	0.08 (0.06)	0.61 (0.35)	0.43 (0.34)	
	Occipital lobe	**0.04** (0.04)	**0.10** (0.03)	**0.10** (0.05)	MixD vs. SVaD: 0.92 **MixD vs. AD: 0.026**
	Temporal lobe	0.01 (0.01)	0.04 (0.04)	0.04 (0.06)	
T1-HypoWMSA, adjusted for ICV volume [% of ICV]	Total white matter	**0.05** (0.05)	**0.34** (0.18)	**0.17** (0.17)	**MixD vs. SVaD: 0.04** **MixD vs. AD: 0.01**
	Frontal lobe	**0.01** (0.01)	**0.15** (0.11)	**0.04** (0.06)	**MixD vs. SVaD: 0.02** **MixD vs. AD: 0.02**
	Parietal lobe	0.002 (0.002)	0.02 (0.02)	0.02 (0.04)	
	Occipital lobe	0.003 (0.004)	0.008 (0.007)	0.02 (0.02)	
	Temporal lobe	0.0005 (0.0007)	0.002 (0.003)	0.002 (0.004)	

*Pairwise comparisons were conducted only if omnibus F-test was significant at p < 0.05. Pairwise p-values were corrected for multiple comparisons using Dunnett's post hoc test with MixD as the control group. Subgroup comparisons were adjusted for age and sex.
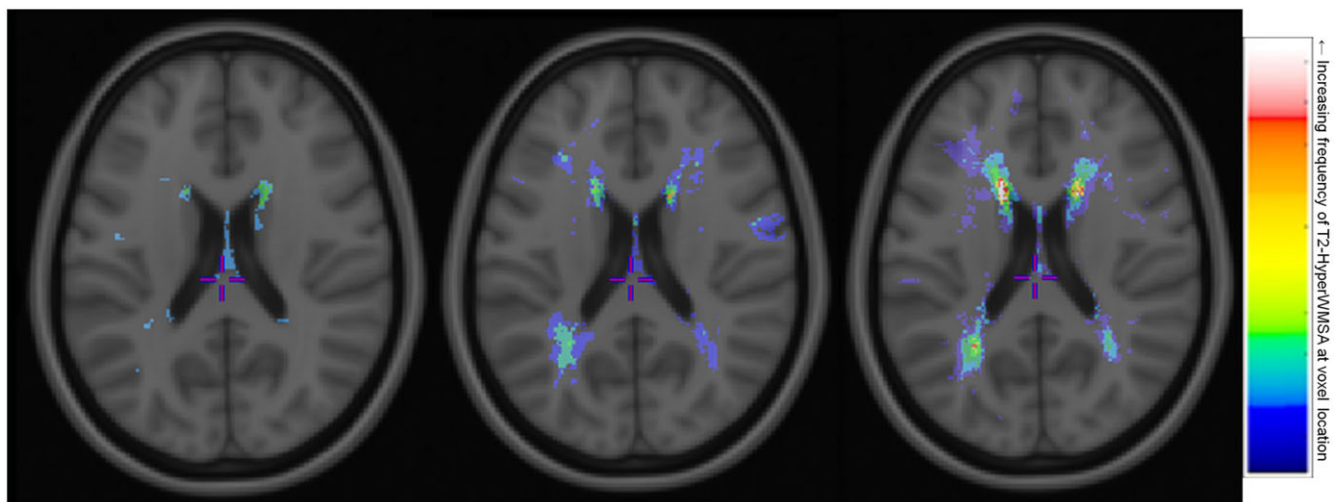
Figure 3: Frequency maps of T2-HyperWMSA for AD (Left), SVaD (Middle), and MixD (Right). The maps are spatially normalized to the MNI152 template.

MRI – White-matter Signal Abnormalities

T1-HypoWMSA was able to differentiate MixD from both AD and SVaD, indicating a higher burden of presumably more severely injured tissue in terms of lower signal on T1-weighted MRI. It is unlikely that these T1-HypoWMSA represented cavitated lacunes, which appear hypointense on T2-FLAIR images and were not included in the T2-HyperWMSA masks. Potential sources of T1-HypoWMSA could have included recent small subcortical infarcts or microbleeds associated with cerebral amyloid angiopathy (CAA),[64] both of which are prominent in MixD.

Furthermore, the pathological specificity of hypointensities on T1 gradient-echo sequences (including ours) is relatively low, unlike those on spin-echo sequence which have been histopathologically validated as a marker of severe tissue destruction.[65] Further work is warranted to evaluate the clinical relevance of the hypointensity-based measure, including its origin and association with cognitive impairment.

The MixD subgroup had significantly higher overall burden of T2-HyperWMSA compared to AD and marginally but not significantly higher compared to SVaD. It is known that AD and VaD

Table 4: Diffusion tensor imaging measures within WMSA and normal-appearing white-matter regions of interest

Measure	ROI	Subgroup mean±SD			Pairwise post hoc comparisons p-value *
		AD	MixD	SVaD	
WM DTI Fractional anisotropy (FA)	JHU WM tracts (all regions)	**0.46 (0.030)**	**0.44 (0.013)**	**0.40 (0.034)**	**MixD vs. SVaD: 0.017** MixD vs. AD: 0.36
	JHU WM tracts (NAWM only)	**0.46 (0.029)**	**0.45 (0.010)**	**0.41 (0.032)**	**MixD vs. SVaD: 0.0082** MixD vs. AD: 0.91
	JHU WM tracts (T2-HyperWMSA only)	0.31 (0.19)	0.35 (0.035)	0.29 (0.028)	
WM DTI Mean diffusivity (MD) [mm²/s]	JHU WM tracts (all regions)	0.00094 (0.000083)	0.00099 (0.000059)	0.00099 (0.000080)	
	JHU WM tracts (NAWM only)	0.00094 (0.000081)	0.00097 (0.000055)	0.00098 (0.000074)	
	JHU WM tracts (T2-HyperWMSA only)	0.0010 (0.00064)	0.0011 (0.000062)	0.0012 (0.00013)	

*Pairwise comparisons were conducted only if omnibus F-test was significant at p < 0.05. Pairwise p-values were corrected for multiple comparisons using Dunnett's post hoc test with MixD as the control group. Subgroup comparisons were adjusted for age and sex.

Table 5: Quantitative susceptibility mapping and R2* relaxation measures within WMSA and subcortical structures regions of interest

Measure	ROI	Subgroup mean±SD			Pairwise post hoc comparisons p-value *
		AD	MixD	SVaD	
Quantitative susceptibility mapping (QSM) [ppm]	T2-HyperWMSA	0.00074 (0.0023)	−0.0050 (0.0055)	−0.0022 (0.0058)	
	T1-HypoWMSA	0.011 (0.015)	0.0058 (0.012)	0.0076 (0.017)	
	Caudate	0.020 (0.034)	0.026 (0.023)	0.031 (0.014)	
	Putamen	0.062 (0.028)	0.061 (0.018)	0.052 (0.039)	
	Pallidus	0.12 (0.024)	0.11 (0.029)	0.017 (0.099)	
	Thalamus	−0.024 (0.0075)	−0.023 (0.0099)	−0.018 (0.0044)	
	Hippocampus/ amygdala	0.009 (0.020)	0.011 (0.017)	0.003 (0.020)	
R2* Relaxation rate [hz]	T2-HyperWMSA	**15.6 (1.3)**	**14.6 (1.1)**	**15.0 (0.7)**	**MixD vs. SVaD: 0.04** **MixD vs. AD: 0.03**
	T1-HypoWMSA	9.9 (3.5)	10.1 (1.1)	10.9 (1.3)	
	Caudate	23.6 (3.9)	22.9 (4.2)	23.2 (6.0)	
	Putamen	30.4 (9.5)	30.0 (4.3)	30.7 (9.6)	
	Pallidus	41.6 (7.7)	43.1 (8.2)	47.0 (14.9)	
	Thalamus	21.5 (1.2)	19.8 (2.2)	20.9 (0.8)	
	Hippocampus/ amygdala	17.7 (3.7)	16.9 (2.3)	16.1 (1.4)	

*Pairwise comparisons were conducted only if omnibus F-test was significant at p < 0.05. Pairwise p-values were corrected for multiple comparisons using Dunnett's post hoc test with MixD as the control group. Subgroup comparisons were adjusted for age and sex.
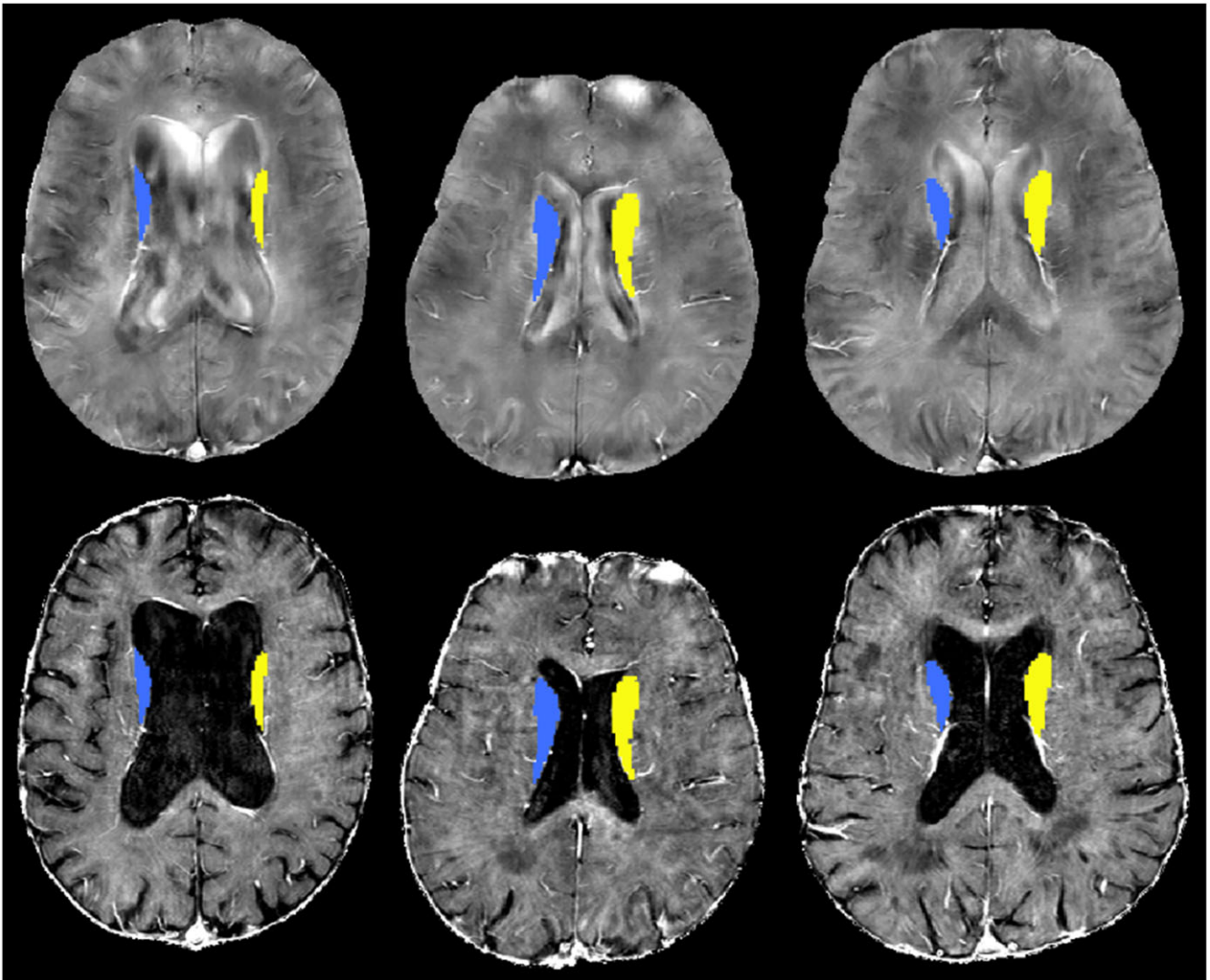
Figure 4: Examples of the QSM (top row) and R2* (bottom row) images from AD (Left), SVaD (Middle), and MixD (Right) participants. Subcortical nuclei masks are overlaid in blue and yellow colors.

have characteristic regional distributions of WM hyperintensities, with different localizations of hyperintensities associated with cognitive impairment as well as conversion to dementia.[66–68] In our AD subgroup, the occipital, parietal, and frontal lobes were more affected by T2-HyperWMSA. This is consistent with the findings of higher posterior preponderance (e.g. posterior periventricular and the splenium of the corpus callosum),[66] as well as frontal lobar burden in AD.[67–69]

For VaD, studies have shown increased burden of WM hyperintensities in the frontal and parietal lobes,[68] which is likely related to the anterior preponderance of WM hyperintensities in ischemic stroke patients.[70,71] Moreover, posterior cerebral artery territories are also affected after ischemic stroke,[70] contributing to the heterogeneous nature of VaD. Accordingly, the parietal, frontal, and occipital lobes were mostly affected by T2-HyperWMSA in our SVaD subgroup.

Our MixD subgroup was characterized by the greatest T2-HyperWMSA burden, which were most prominent in the frontal and parietal WM lobes, accounting for around 1.2% and 0.6% of the ICV, respectively. Intriguingly, the frontal lobe involvement, in terms of T1-HypoWMSA, was significantly greater compared to

both SVaD and AD. Whether this implies AD- or CAA-mediated exacerbation of vascular disturbances requires further verification, as WM abnormalities on MRI can represent different underlying etiologies. Future work is warranted to determine if the subgroups have different types or accelerated time courses of vascular events.

MRI – DTI

Microstructural WM tissue properties were assessed using DTI parameters FA and MD. It is known that FA is reduced and MD is elevated in aging-related WM hyperintensities compared to NAWM,[72] rendering it a non-specific marker of WM injury associated with axonal damage, demyelination, gliosis, or inflammation. As such, widespread DTI abnormalities have been reported in SVaD relative to AD, especially in the genu of the corpus callosum and prefrontal cortex WM tracts (e.g. anterior thalamic radiations and inferior fronto-occipital fasciculi).[25,73–75] On the other hand, in AD, temporal lobe, hippocampus, and the splenium of the corpus callosum are more affected than in SVaD.[25,75] Therefore, it was unexpected that our MixD, with extensive WM hyperintensities, resembled

AD in terms of DTI parameters with significantly higher FA and marginally lower MD values within NAWM compared to SVaD. Several factors may explain this finding. First, progression of brain atrophy or WM lesion formation is related to loss of WM microstructural integrity, such that decreases in FA and increases in MD can be observed in "vulnerable" NAWM regions that are likely to convert into WM lesions (e.g. hyperintensities on T2-FLAIR) in the future.[76] This is a dynamic process, and it is possible that our MixD and SVaD subgroups were in different stages in terms of ongoing cerebrovascular events. For example, our SVaD participants may have had a higher average proportion of vulnerable normal-appearing WM compared to MixD, and this would have led to reduced FA in SVaD at the time of MRI visits. Second, different levels of extracellular fluid accumulation, due to vasogenic edema or other factors, may have confounded the DTI estimates. For example, a recent study suggested that "free water (FW)", a DTI-based proxy for tissue water content, is increased in NAWM of VaD and MixD compared to AD or healthy controls.[77] It is possible that edema accumulation may have applied pressure to adjacent WM fibers, resulting in a denser parallel alignment and a concomitant, arbitrary increase in FA.[78] Third, the effect of crossing-fibers on FA values might have been different between MixD and SVaD, due to different regional distribution of WM hyperintensities that affect the crossings, or different pattern of degeneration of fiber bundles that constitute the crossings. A future longitudinal study will be helpful to identify these WM changes and to determine whether the pattern of progression differs between SVaD and MixD or AD.

MRI – QSM and R2*

Previous studies have reported abnormally elevated susceptibility values in AD, VaD, and subcortical vascular MCI, particularly within the caudate, putamen, and hippocampus, compared to healthy controls.[27,28,31] Although we did not have healthy controls to compare against, the susceptibility measures were likely elevated in all of our participants due to AD or vascular-related pathology. We did not observe group differences in susceptibility within the test subcortical nuclei structures, which is in line with a previous comparison where the authors did not observe significant subcortical QSM differences between AD and VaD.[27] These findings suggest that a similar level of iron accumulation within the assessed subcortical ROIs is present in all three dementia subtypes, even though the mechanisms of the accumulation may differ. For example, the QSM values in AD and MixD may have been influenced by amyloid accumulation and neurofibrillary tangles.[79,80]

Within T2-HyperWMSA, the MixD subgroup had significantly lower R2* compared to both AD and SVaD, while the group differences in the QSM values were nonsignificant. As tissue water content is strongly negatively associated with R2* but not with QSM, this observation likely represents relatively elevated fluid accumulation (e.g. edema) within the T2-HyperWMSA areas of MixD. Tissue edema is commonly associated with disrupted tissue matrix, microglia activation, and blood–brain barrier (BBB) disruption. For instance in AD, CAA is linked to BBB disruption, infarcts, and WM changes, along with inflammatory and immune responses.[81,82] BBB permeability is also increased in people with subcortical vascular disease,[83] where factors like hypoperfusion and thromboembolism lead to inflammatory responses.[84] It is possible that MixD represents an additive or synergistic combination of both conditions, manifesting as a relatively higher degree of edema within the abnormal WM tissue. Whether this actually points to increased neuroinflammatory responses in MixD is not possible to confirm using MRI alone and needs to be verified using peripheral inflammatory biomarkers.[85]

Summary and Study Limitations

Our findings have several implications for future study of imaging markers for MixD. First, most of our MixD participants were also PiB-positive with uptake patterns similar to those observed in AD. This implies that the stratification based on clinical severity is correlated with abnormal amyloid deposition and may corroborate the evaluation of potential MixD cases when amyloid PET imaging is not feasible. Second, an evaluation of tissue integrity-related MRI measures may help better characterize the status of tissue damage in MixD. WMSA observed in our MixD participants may also have been due to causes other than small vessel disease, for example demyelination or inflammatory activity. Our study included DTI and QSM measures, which may represent microstructural changes during demyelination or axonal degeneration. While we did not find strong evidence of DTI changes or elevated QSM within the WMHs of our MixD group, we suggest that potential demyelination within WMSAs needs to be further investigated using MRI measures sensitive to myelin changes, such as myelin water imaging.[86] In addition, T2-HyperWMSAs of our MixD participants had a higher proportion of areas with reduced intensity on T1-weighted images and lower average values on R2* maps. These findings suggest that WMSAs in MixD may be further affected by underlying pathology, such as greater axonal loss and/or fluid accumulation, compared to those in SVaD or AD. Future research will benefit from the inclusion of inflammatory markers in evaluating the implications of imaging data.

There were several limitations to our study. First, our AD, SVaD, and MixD groups were based on clinical diagnoses, but autopsy findings are crucial to confirm the actual presence of mixed pathology. Clinical and neuropathological diagnoses are not necessarily correlated,[87,88] and we cannot exclude that some of our participants could have been misclassified. Second, the clinical diagnosis criteria used in our study included visual rating scales of periventricular and deep white-matter hyperintensities.[39,40] This implies that our SVaD and MixD groups were classified based on the same imaging criteria, and therefore, the total T2-HyperWMSA burden would have been "pre-destined" to possess less sensitivity to distinguish the two groups. We have alleviated this limitation by investigating the lobar distribution of WMSA volumes, which detail location and size of WM lesions, as well as incorporating the T1-HypoWMSA, which may be more specific to tissue damage in the WM. Third, we acknowledge that our sample size was very small and our findings should be interpreted with caution. While we presented imaging characteristics of our MixD group using various MRI contrasts and methods, it is likely that some of the comparisons did not have sufficient power to detect true between-group differences. Yet, we believe that our exploratory findings can provide practical a priori information for future studies investigation MixD population. Fourth, MixD likely represents a heterogeneous spectrum that depends on the relative influence of and interaction between AD and cerebrovascular pathologies.[89] However, the small sample size prevented us from including a subgroup interaction term in the statistical models, which would be necessary to examine the possible synergistic exacerbation of abnormalities in MixD. Also, a larger sample size is necessary to evaluate the correlation between imaging and

neuropsychological findings, especially those involving region-specific or domain-specific measures. Given the practical difficulties of recruiting participants with suspected MixD, a multi-site pooling of data may be required to conduct these types of analyses. Fifth, several participants were missing PiB-PET scans, which prevented us from stratifying participants based on positive/negative PiB-PET binding. Integration of amyloid-specific biomarkers would have reinforced the assignment of the suspected MixD status. Sixth, a longitudinal design is needed to compare the progression of imaging abnormalities, such as whether the conversion of NAWM into WMSA (and the accompanying DTI parameter changes) is accelerated in MixD. The same design is also favored to track the rates of brain atrophy that may be additionally contributed by vascular factors.

Conclusions

Our exploratory analyses suggest that MixD patients present characteristic abnormalities, including higher burden of MRI signal alterations within the frontal lobar areas and potentially elevated tissue water content within the abnormal WM areas than in "pure" AD or SVaD. Future studies are warranted to expand our findings in a larger sample, to investigate the underlying etiologies, and to determine the clinical relevance of these characteristics.

Author Contributions. HL: Conceptualization, Methodology, Software, Formal analysis, Investigation, Writing – Original Draft, Visualization.

VW: Software, Investigation, Writing – Review & Editing, Visualization.

AR: Software, Investigation, Writing – Review & Editing.

CK: Software, Writing – Review & Editing.

MFB: Software, Investigation, Writing – Review & Editing.

KP: Software, Investigation, Writing – Review & Editing.

RT: Software, Investigation, Writing – Review & Editing.

KL: Software, Investigation, Writing – Review & Editing.

CJ: Investigation, Writing – Review & Editing.

VS: Software, Investigation, Writing – Review & Editing.

ES: Software, Investigation, Writing – Review & Editing.

JP: Investigation, Writing – Review & Editing.

GYRH: Conceptualization, Methodology, Investigation, Resources, Writing – Review & Editing, Supervision, Project administration, Funding acquisition.

References

1. Alzheimer's disease facts and figures. Alzheimer's Dement. 2020;16:391–460, 2020.
2. O'Brien JT, Thomas A. Vascular dementia. Lancet. 2015;386:1698–706.
3. Scheltens P, Blennow K, Breteler MMB, et al. Alzheimer's disease. Lancet. 2016;388:505–17.
4. Pantoni L. Cerebral small vessel disease: from pathogenesis and clinical characteristics to therapeutic challenges. Lancet Neurol. 2010;9:689–701.
5. Chui HC, Ramirez-Gomez L. Clinical and imaging features of mixed Alzheimer and vascular pathologies. Alzheimers Res Ther. 2015;7:21.
6. Jørgensen IF, Aguayo-Orozco A, Lademann M, et al. Age-stratified longitudinal study of Alzheimer's and vascular dementia patients. Alzheimer's Dement. 2020;16:908–17.
7. Lee JH, Kim SH, Kim GH, et al. Identification of pure subcortical vascular dementia using 11C-Pittsburgh compound B. Neurology. 2011;77:18–25.
8. Kim HJ, Kim J, Cho H, et al. Individual subject classification of mixed dementia from pure subcortical vascular dementia based on subcortical shape analysis. PLoS One. 2013;8:e75602.
9. Snowdon DA. Brain infarction and the clinical expression of alzheimer disease: the nun study. JAMA J Am Med Assoc. 1997;277:813.
10. Knopman DS, Parisi JE, Boeve BF, et al. Vascular dementia in a population-based autopsy study. Arch Neurol. 2003;60:569–75.
11. Schneider JA, Arvanitakis Z, Bang W, et al. Mixed brain pathologies account for most dementia cases in community-dwelling older persons. Neurology. 2007;69:2197–204.
12. Schneider JA, Arvanitakis Z, Leurgans SE, et al. The neuropathology of probable Alzheimer disease and mild cognitive impairment. Ann Neurol. 2009;66:200–8.
13. Jellinger KA, Attems J. Neuropathological evaluation of mixed dementia. J Neurol Sci. 2007;257:80–7.
14. Troncoso JC, Zonderman AB, Resnick SM, et al. Effect of infarcts on dementia in the Baltimore longitudinal study of aging. Ann Neurol. 2008;64:168–76.
15. Matsui Y, Tanizaki Y, Arima H, et al. Incidence and survival of dementia in a general population of Japanese elderly: the Hisayama study. J Neurol Neurosurg Psychiatry. 2008;80:366–70.
16. White L. Brain lesions at autopsy in older Japanese-American men as related to cognitive impairment and dementia in the final years of life: a summary report from the Honolulu-Asia aging study. J Alzheimer's Dis. 2009;18:713–25.
17. De Reuck J, Deramecourt V, Cordonnier C, et al. The incidence of post-mortem neurodegenerative and cerebrovascular pathology in mixed dementia. J Neurol Sci. 2016;366:164–6.
18. Dong Y, Gan DZQ, Tay SZ, et al. Patterns of neuropsychological impairment in Alzheimer's disease and mixed dementia. J Neurol Sci. 2013;333:5–8.
19. Anor CJ, O'Connor S, Saund A, et al. Neuropsychiatric symptoms in Alzheimer disease, vascular dementia, and mixed dementia. Neurodegener Dis. 2017;17:127–34.
20. Kim CH, Seo SW, Kim GH, et al. Cortical thinning in subcortical vascular dementia with negative 11C-PiB PET. J Alzheimers Dis. 2012;31:315–23.
21. Kim HJ, Ye BS, Yoon CW, et al. Cortical thickness and hippocampal shape in pure vascular mild cognitive impairment and dementia of subcortical type. Eur J Neurol. 2014;21:744–51.
22. Fernando MS, Simpson JE, Matthews F, et al. White matter lesions in an unselected cohort of the elderly: molecular pathology suggests origin from chronic hypoperfusion injury. Stroke. 2006;37:1391–8.
23. Smith CD, Johnson ES, Van Eldik LJ, et al. Peripheral (deep) but not periventricular MRI white matter hyperintensities are increased in clinical vascular dementia compared to Alzheimer's disease. Brain Behav. 2016;6:n/a–n/a.
24. Lee S, Viqar F, Zimmerman ME, et al. White matter hyperintensities are a core feature of Alzheimer's disease: evidence from the dominantly inherited Alzheimer network. Ann Neurol. 2016;79:929–39.
25. Fu J-L, Zhang T, Chang C, et al. The value of diffusion tensor imaging in the differential diagnosis of subcortical ischemic vascular dementia and Alzheimer's disease in patients with only mild white matter alterations on T2-weighted images. Acta Radiol. 2012;53:312–7.
26. Kim YJ, Kwon HK, Lee J-M, et al. White matter microstructural changes in pure Alzheimer's disease and subcortical vascular dementia. Eur J Neurol. 2015;22:709–16.
27. Moon Y, Han S-H, Moon W-J. Patterns of brain iron accumulation in vascular dementia and Alzheimer's dementia using quantitative susceptibility mapping imaging. J Alzheimers Dis. 2016;51:737–45.

28. Kim H-G, Park S, Rhee HY, et al. Quantitative susceptibility mapping to evaluate the early stage of Alzheimer's disease. NeuroImage Clin. 2017;16:429–38.

29. Acosta-Cabronero J, Williams GB, Cardenas-Blanco A, et al. In vivo quantitative susceptibility mapping (QSM) in Alzheimer's disease. PLoS One. 2013;8:e81093.

30. Tiepolt S, Schäfer A, Rullmann M, et al. Quantitative susceptibility mapping of amyloid-β aggregates in Alzheimer's disease with 7T MR. J Alzheimer's Dis. 2018;64:393–404.

31. Sun Y, Ge X, Han X, et al. Characterizing brain iron deposition in patients with subcortical vascular mild cognitive impairment using quantitative susceptibility mapping: a potential biomarker. Front Aging Neurosci. 30 March 2017;9, 10.3389/fnagi.2017.00081.

32. Haacke EM, Cheng NYC, House MJ, et al. Imaging iron stores in the brain using magnetic resonance imaging. Magn Reson Imaging. 2005;23:1–25.

33. Damulina A, Pirpamer L, Soellradl M, et al. Cross-sectional and longitudinal assessment of brain iron level in Alzheimer disease using 3-T MRI. Radiology. 2020;296:619–26.

34. Ke Y, Qian ZM. Iron misregulation in the brain: a primary cause of neurodegenerative disorders. Lancet Neurol. 2003;2:246–53.

35. Hernández-Torres E, Wiggermann V, Machan L, et al. Increased mean R2* in the deep gray matter of multiple sclerosis patients: have we been measuring atrophy? J Magn Reson Imaging. 2019;50:201–8.

36. Du A-T, Schuff N, Chao LL, et al. White matter lesions are associated with cortical atrophy more than entorhinal and hippocampal atrophy. Int Congr Ser. 2006;1290:89–100.

37. Jagust WJ, Zheng L, Harvey DJ, et al. Neuropathological basis of magnetic resonance images in aging and dementia. Ann Neurol. 2008;63:72–80.

38. Rosenberg GA, Prestopnik J, Knoefel J, et al. A multimodal approach to stratification of patients with dementia: selection of mixed dementia patients prior to autopsy. Brain Sci. 2019;9:187.

39. McKhann GM, Knopman DS, Chertkow H, et al. The diagnosis of dementia due to Alzheimer's disease: recommendations from the National Institute on Aging-Alzheimer's Association workgroups on diagnostic guidelines for Alzheimer's disease. Alzheimers Dement. 2011;7:263–9.

40. Erkinjuntti T, Inzitari D, Pantoni L, et al. Research criteria for subcortical vascular dementia in clinical trials. J Neural Transm Suppl. 2000;59:23–30.

41. Woods RP, Cherry SR, Mazziotta JC. Rapid automated algorithm for aligning and reslicing PET images. J Comput Assist Tomogr. 1992;16:620–33.

42. Fischl B, Dale AM. Measuring the thickness of the human cerebral cortex from magnetic resonance images. Proc Natl Acad Sci. 2000;97:11050–5.

43. Fischl B, Salat DH, Busa E, et al. Whole brain segmentation: automated labeling of neuroanatomical structures in the human brain. Neuron. 2002;33:341–55.

44. Beg MF, Miller MI, Trouvé A, et al. Computing large deformation metric mappings via geodesic flows of diffeomorphisms. Int J Comput Vis. 2005;61:139–57.

45. Khan AR, Wang L, Beg MF. FreeSurfer-initiated fully-automated subcortical brain segmentation in MRI using large deformation diffeomorphic metric mapping. Neuroimage. 2008;41:735–46.

46. Ma D, Popuri K, Bhalla M, et al. Quantitative assessment of field strength, total intracranial volume, sex, and age effects on the goodness of harmonization for volumetric analysis on the ADNI database. Hum Brain Mapp. 2019;40:1507–1527.

47. Jenkinson M, Bannister P, Brady M, et al. Improved optimization for the robust and accurate linear registration and motion correction of brain images. Neuroimage. 2002;17:825–41.

48. Riphagen JM, Gronenschild EHBM, Salat DH, et al. Shades of white: diffusion properties of T1- and FLAIR-defined white matter signal abnormalities differ in stages from cognitively normal to dementia. Neurobiol Aging. 2018;68:48–58.

49. Dadar M, Maranzano J, Ducharme S, et al. White matter in different regions evolves differently during progression to dementia. Neurobiol Aging. 2019;76:71–9.

50. Desikan RS, Ségonne F, Fischl B, et al. An automated labeling system for subdividing the human cerebral cortex on MRI scans into gyral based regions of interest. Neuroimage. 2006;31:968–80.

51. Jenkinson M, Beckmann CF, Behrens TEJ, et al. FSL. Neuroimage. 2012;62:782–90.

52. Behrens TEJ, Woolrich MW, Jenkinson M, et al. Characterization and propagation of uncertainty in diffusion-weighted MR imaging. Magn Reson Med. 2003;50:1077–88.

53. Mori S, Oishi K, Jiang H, et al. Stereotaxic white matter atlas based on diffusion tensor imaging in an ICBM template. Neuroimage. 2008;40:570–82.

54. Hu XY, Rajendran L, Lapointe E, et al. Three-dimensional MRI sequences in MS diagnosis and research. Mult Scler. 2019;25:1700–9.

55. Kames C, Wiggermann V, Rauscher A. Rapid two-step dipole inversion for susceptibility mapping with sparsity priors. Neuroimage. 2018;167:276–83.

56. Denk C, Rauscher A. Susceptibility weighted imaging with multiple echoes. J Magn Reson Imaging. 2010;31:185–91.

57. Fernández-Seara MA, Wehrli FW. Postprocessing technique to correct for background gradients in image-based R*(2) measurements. Magn Reson Med. 2000;44:358–66.

58. Mormino EC, Kluth JT, Madison CM, et al. Episodic memory loss is related to hippocampal-mediated beta-amyloid deposition in elderly subjects. Brain. 2009;132:1310–23.

59. Villemagne VL, Chételat G. Neuroimaging biomarkers in Alzheimer's disease and other dementias. Ageing Res Rev. 2016;30:4–16.

60. Rowe CC, Villemagne VL. Brain amyloid imaging. J Nucl Med Technol. 2013;41:11–8.

61. Laforce R, Rabinovici GD. Amyloid imaging in the differential diagnosis of dementia: review and potential clinical applications. Alzheimers Res Ther. 2011;3:31.

62. Yasuno F, Kajimoto K, Ihara M, et al. Amyloid β deposition in subcortical stroke patients and effects of educational achievement: a pilot study. Int J Geriatr Psychiatry. 2019;34:1651–7.

63. Jang H, Park J-Y, Jang YK, et al. Distinct amyloid distribution patterns in amyloid positive subcortical vascular cognitive impairment. Sci Rep. 2018;8:16178.

64. Wardlaw JM, Smith EE, Biessels GJ, et al. Neuroimaging standards for research into small vessel disease and its contribution to ageing and neurodegeneration. Lancet Neurol. 2013;12:822–38.

65. van Walderveen MA, Kamphorst W, Scheltens P, et al. Histopathologic correlate of hypointense lesions on T1-weighted spin-echo MRI in multiple sclerosis. Neurology. 1998;50:1282–8.

66. Yoshita M, Fletcher E, Harvey D, et al. Extent and distribution of white matter hyperintensities in normal aging, MCI, and AD. Neurology. 2006;67:2192–8.

67. Mortamais M, Reynes C, Brickman AM, et al. Spatial distribution of cerebral white matter lesions predicts progression to mild cognitive impairment and dementia. PLoS One. 2013;8:e56972.

68. Gootjes L, Teipel SJ, Zebuhr Y, et al. Regional distribution of white matter hyperintensities in vascular dementia, Alzheimer's disease and healthy aging. Dement Geriatr Cogn Disord. 2004;18:180–8.

69. Holland CM, Smith EE, Csapo I, et al. Spatial distribution of white-matter hyperintensities in Alzheimer disease, cerebral amyloid angiopathy, and healthy aging. Stroke. 2008;39:1127–33.

70. Schirmer MD, Giese A-K, Fotiadis P, et al. Spatial signature of white matter hyperintensities in stroke patients. Front Neurol. 19 March 2019;10, 10.3389/fneur.2019.00208 Epub ahead of print.

71. Wen W, Sachdev PS. Extent and distribution of white matter hyperintensities in stroke patients. Stroke. 2004;35:2813–9.

72. Maniega SM, Valdés Hernández MC, Clayden JD, et al. White matter hyperintensities and normal-appearing white matter integrity in the aging brain. Neurobiol Aging. 2015;36:909–18.

73. Sugihara S, Kinoshita T, Matsusue E, et al. Usefulness of diffusion tensor imaging of white matter in alzheimer disease and vascular dementia. Acta Radiol. 2004;45:658–63.

74. Zarei M, Damoiseaux JS, Morgese C, et al. Regional white matter integrity differentiates between vascular dementia and Alzheimer disease. Stroke. 2009;40:773–9.

75. Palesi F, De Rinaldis A, Vitali P, et al. Specific patterns of white matter alterations help distinguishing Alzheimer's and vascular dementia, , Front Neurosci. 25 April 2018;12, 10.3389/fnins.2018.00274 Epub ahead of print.

76. Vernooij MW, de Groot M, van der Lugt A, et al. White matter atrophy and lesion formation explain the loss of structural integrity of white matter in aging. Neuroimage. 2008;43:470–7.

77. Ji F, Pasternak O, Liu S, et al. Distinct white matter microstructural abnormalities and extracellular water increases relate to cognitive impairment in Alzheimer's disease with and without cerebrovascular disease. Alzheimers Res Ther. 2017;9:63.

78. Pasternak O, Sochen N, Gur Y, et al. Free water elimination and mapping from diffusion MRI. Magn Reson Med. 2009;62:717–30.

79. Spotorno N, Acosta-Cabronero J, Stomrud E, et al. Relationship between cortical iron and tau aggregation in Alzheimer's disease. Brain. 2020;143:1341–9.

80. Ayton S, Fazlollahi A, Bourgeat P, et al. Cerebral quantitative susceptibility mapping predicts amyloid-β-related cognitive decline. Brain. 2017; 140:2112–9.

81. Sweeney MD, Sagare AP, Zlokovic BV. Blood-brain barrier breakdown in Alzheimer disease and other neurodegenerative disorders. Nat Rev Neurol. 2018;14:133–50.

82. Magaki S, Tang Z, Tung S, et al. The effects of cerebral amyloid angiopathy on integrity of the blood-brain barrier. Neurobiol Aging. 2018;70:70–7.

83. Taheri S, Gasparovic C, Huisa BN, et al. Blood-brain barrier permeability abnormalities in vascular cognitive impairment. Stroke. 2011;42:2158–63.

84. Venkat P, Chopp M, Chen J. Models and mechanisms of vascular dementia. Exp Neurol. 2015;272:97–108.

85. Park J-C, Han S-H, Mook-Jung I. Peripheral inflammatory biomarkers in Alzheimer's disease: a brief review. BMB Rep. 2020;53:10–9.

86. MacKay AL, Laule C. Magnetic resonance of myelin water: an in vivo marker for myelin. Brain Plast. 2016;2:71–91.

87. Brayne C, Richardson K, Matthews FE, et al. Neuropathological correlates of dementia in over-80-year-old brain donors from the population-based Cambridge City over-75s cohort (CC75C) study. J Alzheimer's Dis. 2009;18:645–58.

88. Savva GM, Wharton SB, Ince PG, et al. Age, neuropathology, and dementia. N Engl J Med. 2009;360:2302–9.

89. Emrani S, Lamar M, Price CC, et al. Alzheimer's/vascular spectrum dementia: classification in addition to diagnosis. J Alzheimer's Dis. 2020;73:63–71.